

# Role of Material Properties and Drawing Conditions in the Fabrication of Microstructured Optical Fibers

S. C. Xue, M. C. J. Large, G. W. Barton, R. I. Tanner, L. Poladian, and R. Lwin

**Abstract**—In drawing microstructured optical fibers (MOFs), the cross-sectional hole structure, including holes' relative size and shape, in a finished fiber drawn down from a preform can be different from that designed in the preform due to combined effects of draw tension and surface tension. As a result, the fiber's optical properties relative to the initial design can be significantly altered. In order to find means of minimizing or exploiting hole deformation so that MOFs with desirable optical functionality can be fabricated, the underlying mechanism of hole deformation is analyzed by numerically investigating the continuous draw process of MOFs of different materials under different drawing conditions. It is found that three dimensionless numbers, i.e., 1) the capillary number (related to material properties), 2) the draw ratio, and 3) the aspect ratio (both related to the drawing conditions), can be used to predict the type of hole deformation. Silica and polymer materials are considered in particular, but the use of these dimensionless numbers allows the analysis to be applied to any other material.

**Index Terms**—Fiber fabrication, holey fibers, microstructured optical fibers (MOFs), numerical modeling.

## I. INTRODUCTION

**M**ICROSTRUCTURED optical fibers (MOFs; also known as photonic crystal fibers [1] or holey fibers) made from a single material (either silica [2] or polymer [3]) have been referred to as a new generation of fibers. Their optical effects can be tailored by simply changing the hole pattern in the preform (see Fig. 1, where a silica MOF having a typical hexagonal arrangement of holes is shown) from which the MOFs are drawn down. This attractive feature lends these novel fibers' enormous potential in a diversity of applications.

However, from a manufacturing point of view, it can be difficult to maintain the initial cross-sectional hole structure (both the relative size and shape of holes) in a finished MOF (typically, 100–250  $\mu\text{m}$  in diameter) drawn down from a microstructured preform (typically, 10–25 mm in diameter) after



Fig. 1. Silica MOF having a typical hexagonal arrangement of holes (photograph courtesy of the Optical Fibre Technology Centre).

experiencing substantial extensional deformation under draw tension applied at the draw end. Indeed, it has been experimentally observed [3] and numerically predicted [4], [5] that during drawdown of MOFs, a range of hole deformation patterns can occur, including the following:

- 1) hole collapse, i.e., the hole is partially or totally closed;
- 2) hole expansion, i.e., relative to fiber outer diameter, the hole diameter is increased;
- 3) hole enlargement, i.e., relative to its original size, the hole diameter is absolutely increased;
- 4) hole shape changes, i.e., originally, the circular hole may become noncircular.

Such deformations may lead to a significant alteration of the fiber's optical properties. Changes in the relative size and spacing of the holes will affect the fiber's confinement loss [6] and may determine whether or not the fiber is single moded [7]. The operation of bandgap fibers, for example, depends critically on the geometry and separation of high index regions, and is sensitive to deformations near the core. On the other hand, changes in hole shape may be exploited to produce important optical effects, such as birefringence [8] or high numerical aperture [9]. Therefore, it is necessary to understand the underlying mechanisms of hole deformation. Ultimately, we hope that this understanding will allow us to improve preform design and to control hole deformation by adjusting the drawing conditions.

Theoretical solutions [10], [11] based on quasi-one-dimensional approximate analysis methods [12], [13] give valuable predictions of the likely impact of surface tension forces and internal pressurization on hole size changes for a centric hole, but they give no insight for eccentrically located holes, or deformation caused by interactions between nearby holes. Furthermore, no information can be obtained from these theoretical

Manuscript received July 6, 2005; revised September 14, 2005. This work was supported by both the Australia Research Council and Cactus Fibre Pty Ltd.

S. C. Xue and R. I. Tanner are with the School of Aerospace, Mechanical and Mechatronic Engineering, University of Sydney, Sydney, NSW 2006, Australia (e-mail: shicheng@aeromech.usyd.edu.au; rit@aeromech.usyd.edu.au).

M. C. J. Large is with the Optical Fibre Technology Centre, University of Sydney, Sydney, NSW 2006, Australia (e-mail: M.Large@ofc.usyd.edu.au).

G. W. Barton and R. Lwin are with the Department of Chemical Engineering, University of Sydney, Sydney, NSW 2006, Australia (e-mail: barton@chem.eng.usyd.edu.au; R.Lwin@ofc.usyd.edu.au).

L. Poladian is with the School of Mathematics and Statistics, University of Sydney, Sydney, NSW 2006, Australia (e-mail: l.poladian@maths.usyd.edu.au).

Digital Object Identifier 10.1109/JLT.2005.862427

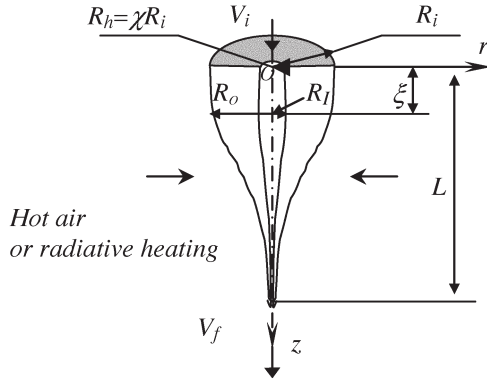


Fig. 2. Schematic diagram of a continuous draw process.

solutions if the extending preform cannot be characterized as a slender body. To understand the drawing processes of MOFs containing arbitrary hole structures, one requires simulations based on computational fluid dynamics.

To our knowledge, only two reported numerical studies are relevant to hole deformation in drawing MOFs. Deflandre [14] investigated thermal effects on periodicity and hole shape in the continuous drawing process, but neither surface tension effects nor draw tension effects were investigated. Xue *et al.* [4], [5] investigated both transient and continuous draw processes of MOFs with some illustrative hole arrangements and included all influential factors with a scaling analysis of the fiber drawing process. They demonstrated that dramatic hole shape changes are expected in drawn MOFs, particularly in the continuous draw process. One of their valuable findings [5] are the conditions for hole size change. They pointed out that surface tension is certainly important in some cases but is not the dominant deformation mechanism for the operating parameters usually used for drawing polymethylmethacrylate (PMMA) MOFs.

In this work, we characterize the drawing process and perform comprehensive numerical investigations for operating parameters covering those used in drawing both silica and PMMA MOFs. We show that different material properties and drawing conditions can produce totally different hole shape changes for the same preform hole pattern. We relate shape changes to hole size variations and show that both can be well characterized by three dimensionless numbers.

## II. PROCESS MODELING

### A. Process Description

Currently, both silica and polymer MOFs are drawn down from preforms using a standard fiber drawing tower [15]. A schematic representation of the continuous draw process is shown in Fig. 2. The original preform of initial radius  $R_i$  is continuously fed into the preheating section of the draw tower at a feed speed  $V_i$ , then passed through the drawing section where it is heated above the glass transition temperature  $T_g$  (for polymer) or the softening point  $T_s$  (for silica) in a cylindrical furnace with the heating wall temperature  $T_w$ . Fiber (with radius  $R_f$ ) is continuously drawn down over a neck-down length  $L$  (i.e., the preform starts contracting at  $z = 0$  and stops contracting at  $z = L$ ) at a draw speed  $V_f (> V_i)$  from the end

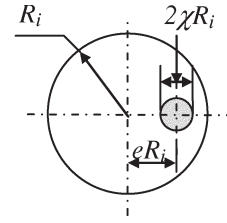


Fig. 3. Cross section of the preform having an eccentric hole.

of the softened preform by applying an appropriate amount of draw tension.

The deformation process from preform to fiber is modeled as a laminar and nonisothermal flow of an incompressible material. The process may be transient (the primary draw for polymer fiber [4] and fiber tapering) or steady state (for the continuous draw process). The basic equations governing such a flow consist of mass, momentum, and energy conservation, and a constitutive relationship for the material rheology. For a Newtonian fluid, all of the equations as well as the proper boundary conditions have been addressed previously [4], [5]. We use a commercial software package (POLYFLOW) [16] based on finite element methods. We have evaluated the accuracy of the package previously [4]. The mesh independence of the numerical solutions has also been assessed.

### B. Process Characterization and Key Parameters

In addition to the draw stability problem existing in traditional fiber draw [17], [18], a new and important issue for fibers containing holes is the question: Can the cross-sectional structure in the drawn fiber be a scaled-down version of that of the preform? Obviously, this is true if and only if there is no variation of the relative size, shape, and position of every hole. Thus, to guide our later numerical analysis, we begin with a qualitative understanding of the important parameters for a fiber containing eccentric holes.

Obviously, hole size is an important parameter and is characterized by the dimensionless ratio  $\chi$  of the initial hole radius  $R_h$  to the outer radius  $R_i$  of the preform.

Size variation of an individual hole is characterized by a collapse ratio [5] expressed as

$$C_o \equiv \frac{R_I(\xi)}{R_o(\xi)}. \quad (1)$$

Here,  $R_I(\xi)$  and  $R_o(\xi)$  are the hole radius and the outer radius of the extending preform at any axial position  $z = \xi$  ( $0 < \xi \leq L$ ), respectively. Thus, collapse occurs if  $C_o < 1$ , the status quo is preserved when  $C_o = 1$ , and hole expansion occurs if  $C_o > 1$ . Hole enlargement can be identified by the condition of  $C_o > R_i/R_o(\xi)$ .

Position variation is characterized by a shift factor  $S_f$ , which is defined as

$$S_f \equiv \frac{e_f}{e}. \quad (2)$$

Here, as shown in Fig. 3,  $e$  and  $e_f$  are the dimensionless position (normalized against  $R_i$ ) of the eccentric hole in the

preform and the final fiber, respectively. Thus, the shift is toward the fiber center if  $S_f < 1$  or toward the fiber boundary if  $S_f > 1$ .

Shape variation is not easily characterized: Depending on the nature of size variations of the individual hole as well as the holes around it, the hole may distort to any shape, such as from a circular one to an ovoid or even a polygon. There is no universal way to characterize the final deformed hole. However, the extent of the shape changes of a hole can still be characterized by using (1) in the two directions where the maximum and minimum expansion or collapse occurs. The greater the difference of  $C_o$  in the two directions, the more dramatic the hole shape change.

We now determine the key parameters that may control these deformations. The overall deformation of an extended preform can be well characterized by two dimensionless parameters, namely 1) the draw ratio defined by the ratio of the draw speeds

$$D_r \equiv \frac{V_f}{V_i} \quad (3)$$

and 2) the aspect ratio defined by

$$\varepsilon \equiv \frac{R_i}{L}. \quad (4)$$

The former characterizes the overall contraction in size and the latter characterizes the overall rate of deformation (contraction amount per unit length) of the extending preform.

In drawing a fiber, inertial, gravitational, and air drag forces are negligible. Thus, in the absence of inner hole pressurization, only two external forces are involved—the draw tension and surface tension forces. The former causes the extensional deformation of a preform, and the latter potentially contributes to the radial contraction. The localized hole deformation is also related to both forces. The draw tension force leads a hole to contract together with the surrounding preform (but not necessarily at the same rate). Meanwhile, curvature-dependent surface tension leads the hole to contract further. The relative importance of these forces is characterized by the localized capillary number defined as

$$C_a \equiv \frac{\eta V_i}{\sigma} \quad (5)$$

where  $\eta$  and  $\sigma$  are the viscosity and the surface tension coefficient of the material, respectively.

The effect of the temperature is implicitly included via the localized temperature-dependent viscosity. For silica, we have Fulcher's law [19], which is written as

$$\eta = 10^{-7.24 + \frac{2.69 \times 10^4}{T}} \text{ Pa} \cdot \text{s} \quad (6)$$

and for PMMA, the measured data for the grade of the PMMA used in our experimental temperature range of 393–483 K give the approximate relation

$$\eta = 0.2661 e^{\frac{2687.8}{(T-273)}} \text{ Pa} \cdot \text{s}. \quad (7)$$

TABLE I  
TYPICAL MATERIAL AND DRAWING PARAMETERS

Parameters	PMMA	Silica
$R_i$ (mm)	5	10
$R_f$ (mm)	$240 \times 10^{-3}$	$62.5 \times 10^{-3}$
$T_w$ (K)	473	2300
$L$ (mm)	20–40	40–50
$V_i$ (mm/min)	2.3	3.0
$V_f$ (m/min)	1.0	76.8
$\eta$ (Pa·s)	$10^5 \sim 10^8$	$10^4 \sim 10^6$
$\sigma$ (N/m)	0.032	0.3
$T_s$ or $T_g$ (K)	393	1900
$\varepsilon$	0.125–0.25	0.2–0.25
$D_r$	$10^2$	$10^4$

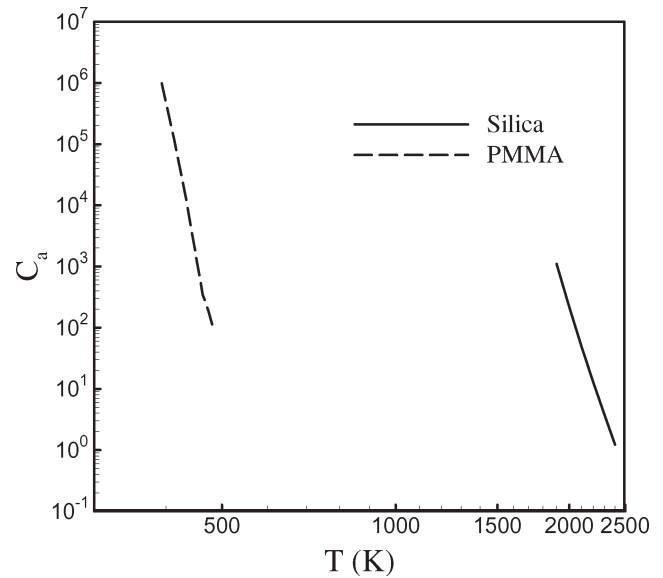


Fig. 4. Capillary number ( $C_a$ ) as a function of the temperature experienced in drawing silica and PMMA fibers.

With the typical operating conditions as listed in Table I, the viscosity (and, thus, capillary number  $C_a$ ) of the material may vary by orders of magnitude due to the range in temperature profiles (from  $T_g$  or  $T_s$  to close to  $T_w$ ). In Fig. 4, we show typical values of  $C_a$  for silica and PMMA for temperatures experienced by an extending preform inside a furnace at a typical feeding speed (i.e.,  $V_i = 2.4$  mm/min). For PMMA,  $C_a$  varies from  $10^6$  to  $10^2$ ; but, for silica, it varies from  $10^3$  to values as low as  $10^0$ . Therefore, even without considering viscoelastic effects [20], the hole deformation behavior can be extremely different for different materials and different heating and drawing conditions. Experimental confirmation of our numerical predictions [4], [5] for simple fibers has demonstrated that viscoelastic effects are less important than surface tension effects. Thus, in this work, we concentrate on the role of  $C_a$  and ignore viscoelastic effects.

We expect the deformation behavior, and, in particular, the collapse ratio is determined by the above three dimensionless parameters and the initial hole size. Thus

$$C_o = f(\varepsilon, D_r, \chi, C_a). \quad (8)$$

Indeed, we have previously derived a specific analytical result for an annular hollow fiber with  $\varepsilon \ll 1$  (slender body) to leading order [11]

$$C_o = 1 - \left(\frac{1}{\chi}\right) \left(\frac{1}{\ln D_r}\right) \left(\frac{1}{\varepsilon}\right) \left(\frac{1}{C_a}\right). \quad (9)$$

However, in practical fiber drawing, an extending preform may not be annular or qualify as a slender body; in such cases, numerical analysis is required. For nonslender annular fibers, Xue *et al.* [5] have quantitatively demonstrated that hole size variation is well described by a relation such as (8) even for aspect ratios of 0.25 over a wide range of parameters. In this paper, we confirm and determine relation (8) by numerical analysis for MOFs with multiple or off-center holes.

C. Nonisothermal Effects

Localized variations of the temperature (and, thus,  $C_a$ ) can affect hole contraction, even when surface tension effects are only included to leading order [4]. In the heating and drawing process, both axial and radial temperature gradients are expected [5], [21]. These gradients are determined by the size of the preform, the air fraction of the hole structure, the feeding speed, and the heat transfer efficiency. Once the temperature at any radial position on a cross-section of the preform reaches  $T_g$  or  $T_s$ , localized hole deformation may occur due to the high sensitivity of the viscosity of the fiber material to the temperature. Hence, it is very important for the preform to be heated up efficiently and symmetrically to avoid any nonuniform hole deformation on the cross-section before the preform starts extending. Similarly, over the deformable section (i.e., neck-down region where substantial contraction occurs), axial temperature gradients lead to variations in  $C_a$ . Meanwhile, the hole size in the extending preform is contracting. Therefore, the relative importance of the viscous forces and the surface tension forces changes along the neck-down region as analyzed by Xue *et al.* [5]. To accurately predict the combined impact of the neck-down shape and variations in  $C_a$ , it is necessary to carry out nonisothermal simulations with accurate data about the thermal properties of the material. However, due to the lack of measured thermodynamic properties and to avoid introducing extra uncertainties, we concentrate on isothermal simulations. Given that surface tension effects reach a maximum at the highest temperature in the preform, we will assume this constant temperature to be 468 K for PMMA and 2073–2173 K for silica, which is well above the deformable temperature of the corresponding material and represents that at a typical feeding speed 2.4 mm/min, orders of magnitude of  $C_a$  are 25–50 and 200 for silica and PMMA, respectively.

III. NUMERICAL ANALYSIS

A. Hole Size Variation of an Eccentric Hole

We begin by simulating the drawing of fibers from a preform of  $R_i = 5$  mm containing one single eccentric hole with  $\chi = 0.05$  and  $e = 0.2$  (see Fig. 3). The results for an eccentric hole are similar to those predicted theoretically [10], [11] and

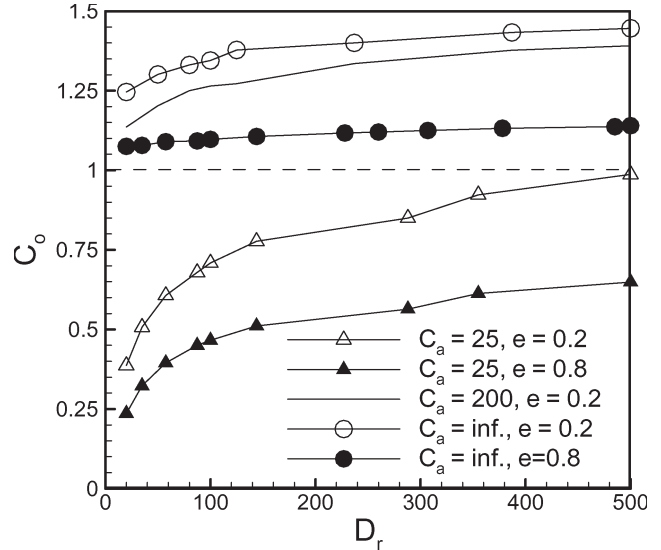


Fig. 5. Collapse ratio as a function of draw ratio for fibers containing an eccentric hole ( $\chi = 0.05$ ) drawn down over a short neck-down length ( $\varepsilon = 0.25$ ). Results are for different capillary numbers ( $C_a$ ) and radial hole positions ( $e$ ).

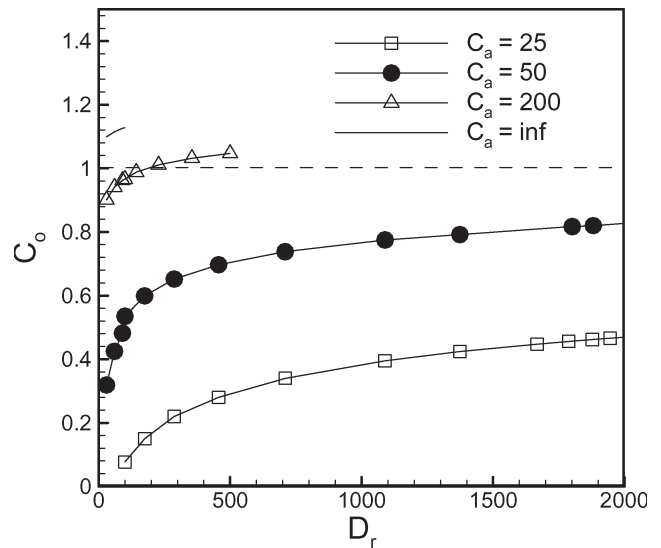


Fig. 6. Similar to Fig. 5 but for a long neck-down length ( $\varepsilon = 0.125$ ).

numerically [5] for a central hole (i.e., an annular fiber). Figs. 5 and 6 show the numerically predicted collapse ratio  $C_o$  as a function of the draw ratio  $D_r$  for two different neck-down lengths and various capillary numbers. Silica is represented by  $C_a = 25$ –50, PMMA is represented by  $C_a = 200$ , and the ignoring surface tension corresponds to  $C_a$  infinite.

As seen in Fig. 5, with a short neck-down length ( $\varepsilon = 0.25$ ) hole expansion ( $C_o > 1$ ) occurs for  $C_a = 200$  (PMMA) and is enhanced by increasing  $D_r$ , while for  $C_a = 25$  (silica), hole collapse ( $C_o < 1$ ) occurs and is reduced by increasing  $D_r$ . On the other hand, as seen in Fig. 6, with a long neck-down length ( $\varepsilon = 0.125$ ), hole collapse dominates, and hole expansion only occurs when  $C_a$  or  $D_r$  is high enough. Both Figs. 5 and 6 demonstrate hole expansion is enhanced and hole collapse is reduced by increasing the draw ratio  $D_r$ .

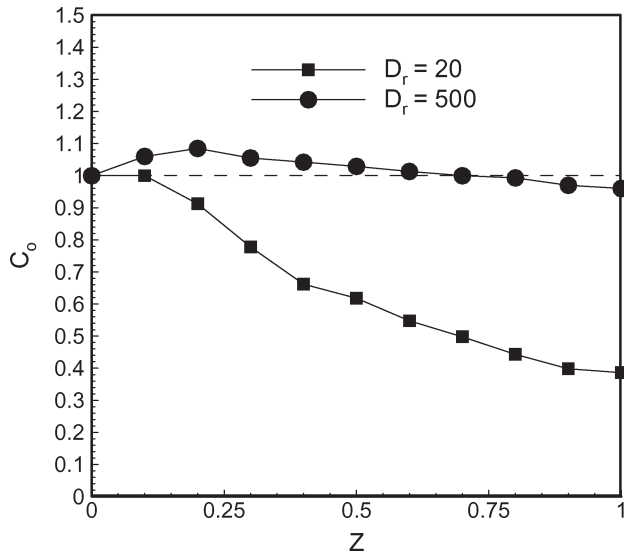


Fig. 7. Profiles of the collapse ratios of an eccentric hole ( $\chi = 0.05$ ,  $e = 0.2$ ) along the draw direction over a long neck-down length ( $\varepsilon = 0.125$ ) for the cases of  $C_a = 25$  at two different draw ratios (i.e.,  $D_r = 20$  and 500).

A particular practical outcome is that it is possible to turn hole collapse to hole expansion by increasing  $D_r$  or using a short neck-down length. As shown in Fig. 5, for  $C_a = 25$  and  $e = 0.2$ , dramatic hole collapse ( $C_o = 0.39$ ) for  $D_r = 20$  can be virtually eliminated ( $C_o = 0.98$ ) by increasing  $D_r$  to 500. Further increases to  $D_r = 6000$  (not shown in Fig. 5) produce hole expansion ( $C_o = 1.24$ ).

The underlying mechanism in controlling hole size is that for a given neck-down length, increasing  $D_r$  leads to a steeper neck-down region, i.e., a greater value of  $|dR_o/dz|$ . Xue *et al.* [5] performed a localized force balance to show that the ratio between the viscous force  $F_{vis}$  induced inside the fiber body and the surface tension force  $F_s$  around a centric hole is

$$\frac{F_{vis}}{F_s} \approx 2 \left| \frac{dR_o}{dz} \right| C_a. \quad (10)$$

This indicates that increasing  $|dR_o/dz|$  has the same function as increasing  $C_a$ . When  $C_a = \infty$ , viscous force is the only force involved and no force acting inward the hole surface (leading to hole collapse). Note that  $|dR_o/dz|$  varies along the draw direction, and much greater  $|dR_o/dz|$  is expected in the upstream portion of the extending preform. Thus, surface tension is less important there, which leads to hole expansion in the upstream portion of the preform. This feature is clearly demonstrated in Fig. 7, which shows the collapse ratios for two different draw ratios (i.e.,  $D_r = 20$  and 500). It confirms that final hole collapse is greatly reduced by increasing  $D_r$ , and the reduction is attributed to hole expansion in the upstream portion (near  $z = 0.25$ ) of the extending preform.

Relation (10) has taken the curvature change along the draw direction into account in evaluating the relative importance of the two forces. Now, for a given draw ratio  $D_r$ , a smaller value of  $\varepsilon$  means more dramatic contraction over a shorter (thus, steeper) neck-down region ( $|dR_o/dz| \gg 1$ ); likewise, for a fixed  $\varepsilon$ , a larger draw ratio also means a greater localized deformation rate in a given neck-down length. Thus, increasing

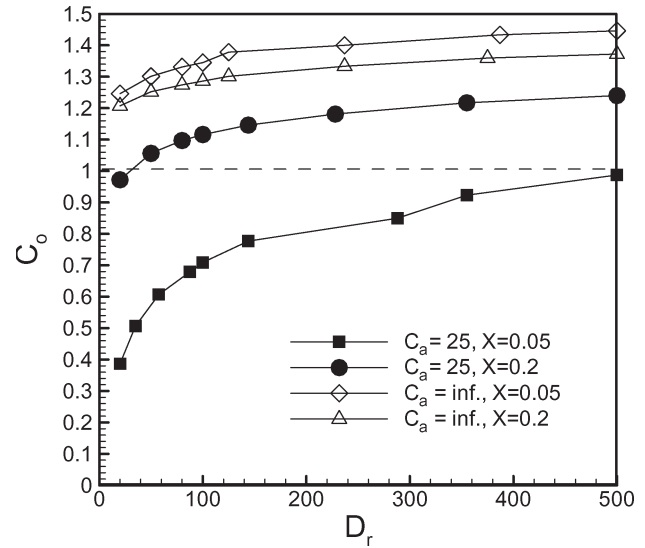


Fig. 8. Collapse ratio as a function of draw ratio at different capillary numbers ( $C_a$ ) for drawing a fiber containing an eccentric hole for two different initial hole sizes (i.e.,  $\chi = 0.05$  and 0.2 with  $e = 0.2$ ).

$D_r$  or decreasing  $\varepsilon$  is equivalent to increasing  $|dR_o/dz|$  and has the same function as increasing  $C_a$ . Thus, (10) incorporates the effects of all three dimensionless numbers. In practical fiber draw,  $D_r$  is fixed by the target final fiber size, thus, it is usually easier to manipulate  $C_a$  or  $\varepsilon$ .

Results without surface tension effects ( $C_a = \infty$ ) show that hole expansion always occurs whenever an extending preform cannot be characterized as a slender body. However, with increasing neck-down length, the extending preform is closer to a slender body (small  $\varepsilon$ ), and the analytical result from (9) is applicable and shows that for  $C_a = \infty$ ,  $C_o$  approaches 1. Previous work [5] and the results here show that surface tension effects can practically be ignored when  $C_a$  exceeds 200.

Now, we check how deformations depend on the initial position ( $e$ ) and the initial hole size ( $\chi$ ). Fig. 5 shows collapse ratios for two different radial positions:  $e = 0.2$  and 0.8. The results show that the collapse ratio is smaller for the hole with a larger  $e$  (further from the center).

Fig. 8 shows the predicted collapse ratio for two different hole sizes located at the same radial location. As seen, regardless of whether hole expansion or hole collapse occurs, the effect is more severe for a smaller hole; in other words,  $C_o$  is further from 1 when  $\chi$  is smaller.

Finally, we consider variation in the position  $S_f$  of an eccentric hole. Our numerical predictions for two different initial hole sizes ( $\chi = 0.05$  and 0.2) and positions (i.e.,  $e = 0.2$  and 0.8) reveal that the dimensionless displacement of the hole center is less than 1% and is inward ( $S_f < 1$ ), as expected for a contracting preform. Thus, shifts in position are negligible for isolated holes. For MOFs containing multiple holes, interaction between nearby holes may lead to larger shifts. In this paper, we concentrate on shape changes produced by nearby holes and leave the analysis of the more subtle shift in position to future work together with determining the critical edge-to-edge distance between holes at which the interactions between holes can be avoided in drawing MOFs.

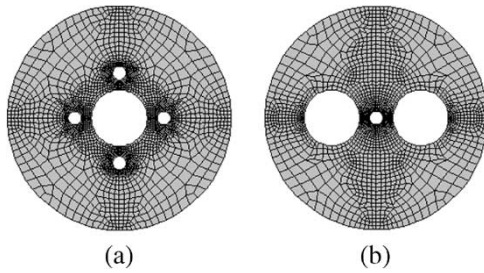


Fig. 9. Initial cross-sectional hole structures in (a) five-hole and (b) Panda preforms.

### B. Hole Shape Changes Due to Interactions Between Holes

The predictions above for a single eccentric hole reveal that the different forms (expansion or collapse) of hole size variations are well characterized by the three dimensionless numbers  $C_a$ ,  $\varepsilon$ , and  $D_r$ . In this section, we will show that deformations caused by the interactions between neighboring holes are also characterized by these same three numbers. Simulations will be carried out for the two illustrative cross-sectional hole structures shown in Fig. 9.

In the five-hole structure [Fig. 9(a)], four small “satellite” holes are symmetrically located around a large central circular hole with the dimensionless pitch  $\Lambda$  (normalized against  $R_i$ ) between hole centers being 0.4. The dimensionless radii  $\chi$  (normalized against  $R_i$ ) for the small and large holes are 0.05 and 0.3, respectively. In the “Panda” structure [Fig. 9(b)], two large holes ( $\chi = 0.3$ ) are symmetrically located around a small central hole ( $\chi = 0.05$ ), again with  $\Lambda = 0.4$ . These structures have been chosen, not only because they (having holes of different size in close proximity) can be expected to display quite large deformations, but also, they are intrinsically interesting. The five-hole structure has the essential features of a photonic bandgap structure, i.e., a large hollow core closely surrounded by much smaller holes. The “Panda” fiber is again a highly simplified version of a meaningful structure. Large holes surrounding a core region have been used for including electrodes so that the fiber can be poled [22] and can also be used to introduce birefringence, either by the stress-optic effect, or in MOFs, by producing ellipticity in the holes [8].

In our numerical modeling, the two preforms are drawn down with fixed  $D_r = 100$  and feed speed  $V_i = 2.4$  mm/min but for two different neck-down lengths ( $\varepsilon = 0.25$  and 0.125) and two different  $C_a$  values (25 and 200). Fig. 10 shows the final hole structures in the fibers drawn down using a short neck-down region ( $\varepsilon = 0.25$ ) for a material with a greater value of  $C_a = 200$  (representing PMMA). The left-hand figure of each pair is scaled to match the initial preform so that we can easily see the relative size and shape changes of the holes. The right-hand figure of each pair is an enlarged view of a smaller hole to reveal the dramatic shape changes. Although some shape change occurs for all holes, it is more remarkable for holes with larger curvature (small holes) and “curvature-matching” features in hole shape changes [5]. A comparison of Fig. 10 with Fig. 9 confirms the predicted dramatic hole expansion.

Shape changes in adjacent holes caused by hole expansion can be explained by a force balance argument. During hole

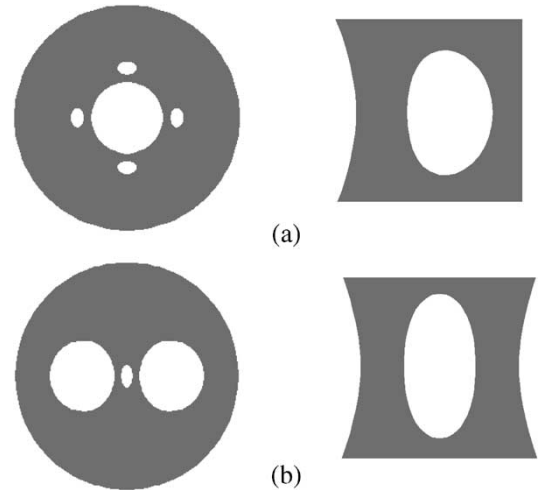


Fig. 10. Pairs of images showing the final hole structures in fibers drawn down from the preform of (a) five-hole and (b) Panda hole structures with  $\varepsilon = 0.25$  at  $C_a = 200$ .

expansion, the hole is contracting relatively slower than the surrounding preform. The difference in the contracting rates leads to compressive forces being formed in the zones between the hole boundary (if a hole is centrally located) and the preform boundary. The compressive forces tend to push the material around the hole away. As a result, any expansion of the holes in these zones and the central hole itself will be partially suppressed in the direction of any nearby hole, while, along boundaries away from nearby holes, the expansion is unaffected. Thus, suppressed expansion in some directions along with the maintained expansion in other directions leads to holes in close proximity becoming noncircular. Because size change is more dramatic for smaller holes, shape changes will likewise be more dramatic for the smaller of two adjacent holes.

For example, for the five-hole structure [see Fig. 10(a)], hole expansion of both the larger central hole and the four “satellite” holes is partially suppressed in directions joining the holes or close to the outer preform boundary, while in directions where there are no nearby holes, such as the azimuthal direction for the four small holes, the hole is expanding freely. The result of this nonuniform expansion is that the four small satellite holes become ovoid with their major axes along the azimuthal direction. Similarly, for the “Panda” hole structure [see Fig. 10(b)], dramatic hole expansion of the central small hole is suppressed in the direction of the two larger expanding holes. As a result, the small hole becomes ovoid with the major axis at right angles to the line joining the two larger holes. In both structures, as expected, the shape change of the larger holes is not as remarkable, showing only slightly suppressed expansion in the directions toward the smaller holes.

Fig. 10 shows results typical for PMMA. However, if these preforms are drawn using a longer neck-down region for a material with a smaller value of  $C_a$ , such as is typical for silica, then, at the same draw ratio, a much smaller draw tension is required, so surface tension effects become more pronounced. Then, as shown in Fig. 11, hole collapse occurs in all holes for both structures. Here, the collapsed smaller holes are too small to resolve with the scale of the figures. However, the

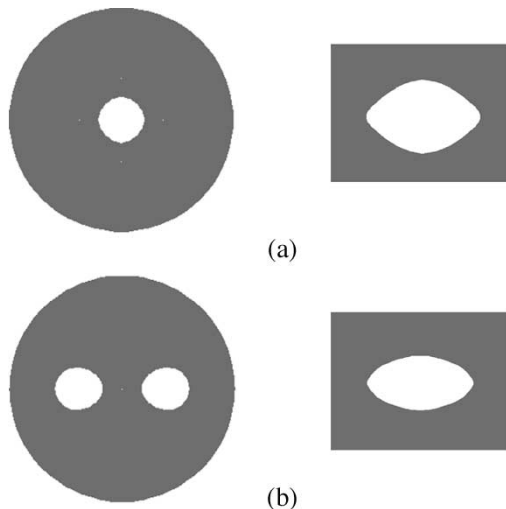


Fig. 11. Pairs of images showing the final hole structures in fibers drawn down from the preform of (a) five-hole and (b) Panda hole structures with  $\varepsilon = 0.125$  at  $C_a = 25$ .

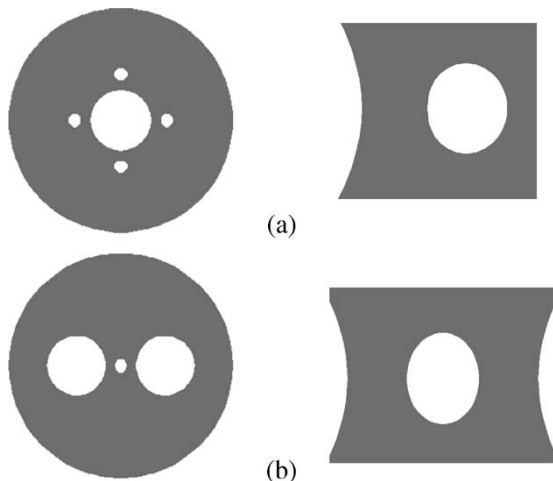


Fig. 12. Pairs of images showing the final hole structures in fibers drawn down from the preform of (a) five-hole and (b) Panda hole structures with  $\varepsilon = 0.125$  at  $C_a = 200$ .

deformation of the smaller holes can be seen in the enlarged right-hand figures of each pair. Comparing Fig. 11 to Fig. 10 clearly shows the dramatic effect of changing material or draw conditions. In this case, the deformed small holes are still ovoid but with major axis toward a neighboring hole.

Again, these deformations can be explained by force balance arguments analogous to those used when hole expansion takes place. During hole collapse, the hole is contracting relatively faster than the surrounding preform. The difference in the contracting rates leads to stretching forces around the holes. These forces tend to pull the surrounding material in. Therefore, the extent of collapse will be partially reduced in the direction of any nearby hole. The reduced collapse in the direction of the neighboring hole along with the maintained collapse in the other directions produces an ovoid shape as shown in Fig. 11.

As mentioned earlier, hole size changes can be reduced by adjusting the neck-down length or the capillary number. The same is true for hole shape changes. For example, deformation caused during hole expansion is reduced by using a longer

neck-down length as seen by comparing Fig. 12 with Fig. 10. Similarly, deformation caused during hole collapse can be reduced by using a shorter neck-down length.

#### IV. CONCLUSION

We have demonstrated that three dimensionless parameters (i.e., capillary number, draw ratio, and aspect ratio) can be used to predict or control hole deformation during the MOF drawing process. In particular, for the two most commonly used materials for MOFs, silica and PMMA, we have shown that quite different deformations can be observed for the same structure under equivalent draw conditions: The silica case is dominated by hole collapse, while for PMMA, hole expansion is more important. For a fixed draw ratio, the capillary number and aspect ratio can be used to compensate for the material properties.

This work is currently purely computational, although previous work [4], [5] has shown that this style of analysis yields conclusions consistent with experimental results. We intend to explicitly test the predictions of this work in the future. Similarly, this paper does not consider the use of pressure (both positive and negative)—another parameter that has been widely used to control structures in MOFs. This will also be considered in future work.

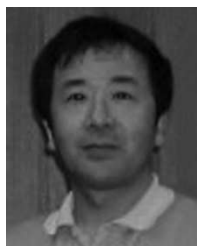
#### ACKNOWLEDGMENT

The authors thank Dr. S. Dai for measuring the material data of the PMMA used and Dr. K. Lytikäinen for supplying the relevant drawing conditions of silica fibers.

#### REFERENCES

- [1] P. F. Russell, "Photonic crystal fibre," *Science*, vol. 299, no. 5605, pp. 358–362, Jan. 2003.
- [2] J. C. Knight, T. A. Birks, R. F. Russell, and D. M. Atkins, "All silica single-mode optical fiber with photonic crystal cladding," *Opt. Lett.*, vol. 21, no. 19, pp. 1547–1549, Oct. 1996.
- [3] M. A. van Eijkelenborg, M. C. J. Large, A. Argyros, J. Zagari, S. Manos, N. A. Issa, I. Bassett, S. Fleming, R. C. McPhedran, C. M. de Sterke, and N. A. P. Nicorovici, "Microstructured polymer optical fibre," *Opt. Express*, vol. 9, no. 7, pp. 319–327, Sep. 2001.
- [4] S. C. Xue, R. I. Tanner, G. W. Barton, R. Lwin, M. C. J. Large, and L. Poladian, "Fabrication of microstructured optical fibres—Part I: Problem formulation and numerical modelling of transient draw process," *J. Lightw. Technol.*, vol. 23, no. 7, pp. 2245–2254, Jul. 2005.
- [5] —, "Fabrication of microstructured optical fibres—Part II: Numerical modelling of steady-state draw process," *J. Lightw. Technol.*, vol. 23, no. 7, pp. 2255–2266, Jul. 2005.
- [6] T. P. White, R. C. McPhedran, C. M. de Sterke, L. C. Botten, and M. J. Steel, "Confinement losses in microstructured optical fibers," *Opt. Lett.*, vol. 26, no. 21, pp. 1660–1662, Nov. 2001.
- [7] B. T. Kuhlmey, R. C. McPhedran, and C. M. de Sterke, "Modal cutoff in microstructured optical fibers," *Opt. Lett.*, vol. 27, no. 19, pp. 1684–1686, Oct. 2002.
- [8] N. A. Issa, M. A. van Eijkelenborg, G. Henry, M. Fellow, and M. C. J. Large, "Fabrication and characterization of microstructured optical fibres with elliptical holes," *Opt. Lett.*, vol. 29, no. 12, pp. 1336–1338, Jun. 2004.
- [9] N. A. Issa, "High numerical aperture in multimode microstructured optical fibers," *Appl. Opt.*, vol. 43, no. 33, pp. 6191–6197, Nov. 2004.
- [10] A. D. F. Fitt, K. Furusawa, T. M. Monroe, C. P. Please, and D. J. Richardson, "The mathematical modeling of capillary for holey fibre manufacture," *J. Eng. Math.*, vol. 43, no. 2–4, pp. 210–227, May 2002.
- [11] S. C. Xue, G. Barton, M. C. J. Large, R. Lwin, L. Poladian, and R. I. Tanner, "Analysis of hole deformation in drawing microstructured

- optical fibres," in *Proc. 13th Int. Plastic Fibres Conf.*, Nürnberg, Germany, Sep. 2004, pp. 269–276.
- [12] M. R. Matovich and J. R. A. Pearson, "Spinning a molten threadline—Steady-state isothermal viscous flows," *Ind. Eng. Chem. Fundam.*, vol. 8, no. 3, pp. 512–520, Aug. 1969.
- [13] W. W. Schultz and S. H. Davis, "One-dimensional liquid fibers," *J. Rheol.*, vol. 26, no. 4, pp. 331–345, Aug. 1982.
- [14] G. Deflandre, "Modeling the manufacturing of complex optical fibres: The case of the holey fibres," in *Proc. 2nd Int. Colloq.*, Valenciennes, France, Jan. 2002, pp. 150–156.
- [15] G. Barton, M. A. van Eijkelenborg, G. Henry, M. C. J. Large, and J. Zagari, "Fabrication of microstructured polymer optical fibres," *Opt. Fiber Technol.*, vol. 10, no. 4, pp. 325–335, May 2004.
- [16] *POLYFLOW User's Manual, ver. 3.10*, Fluent Inc., Lebanon, NH, Sep. 2003.
- [17] A. Ziabicki, *Fundamentals of Fibre Formation*. London, U.K.: Wiley, 1976.
- [18] A. Yarin, P. Gospodinov, and V. I. Rusinov, "Stability loss and sensitivity in hollow fibre drawing," *Phys. Fluids*, vol. 6, no. 4, pp. 1454–1463, Apr. 1994.
- [19] N. P. Bansal and R. H. Doremus, *Handbooks of Glass Properties*. New York: Academic, 1986, p. 680.
- [20] R. I. Tanner, *Engineering Rheology*, 2nd ed. New York: Oxford Univ. Press, 2000, pp. 340–356.
- [21] K. Lyytikäinen, P. Råback, and J. Ruokolainen, "Numerical simulation of a specialty optical fibre drawing process," in *Proc. 4th Int. ASME/JSME/KSME Symp. Computational Technologies Fluid/ Thermal/ Chemical/ Stress Systems Industrial Applications*, S. Kawano and V. V. Kudriavtsev, Eds., Vancouver, BC, Canada, 2002, vol. PVP448-2, pp. 267–275.
- [22] F. Cox, A. Michie, G. Henry, M. Large, S. Ponrathnam, and A. Argyros, "Poling and doping of microstructured polymer optical fibres," in *Proc. 12th Int. Plastic Optical Fibres Conf.*, Seattle, WA, Sept. 14–17, 2003, pp. 89–92.



**S. C. Xue** received the Ph.D. degree in engineering from the University of Sydney, Sydney, NSW, Australia, in 1997.

In 1997, he joined the rheology research group at the School of Aerospace, Mechanical, and Mechatronic Engineering, University of Sydney, and currently works on developing novel numerical methods for solving three-dimensional flow problems involving complex viscoelastic materials. His expertise rang from developing new solution algorithms for differential equation system governing

material transport processes, such as polymer processing, to designing polymer processing machinery and packaging equipment.

**M. C. J. Large** received the B.Sc. degree from the University of Sydney, Sydney, Australia, in 1990 and the Ph.D. degree from Trinity College, Dublin, Ireland, in 1994.

She is now an Australian Research Council Fellow with the Optical Fibre Technology Centre, the University of Sydney, working mostly on microstructured optical fibres.



**G. W. Barton** is currently the Head of Chemical Engineering, University of Sydney, Sydney, NSW, Australia, who has applied his expertise in process systems engineering to an extremely broad range of applications as diverse as cooking extruders and derivative option modeling for financial institutions. His interests in photonics cover the fabrication of both silica and microstructured polymer specialty fibres.



**R. I. Tanner** has been the P. N. Russell Professor of Mechanical Engineering at the University of Sydney, Sydney, NSW, Australia, since 1975, following a nine-year period as a Professor of Engineering at Brown University, Providence, RI. He studies the rheology of materials, especially polymers, and their processing.

Mr. Tanner is a Fellow of the Royal Society of London (FRS).



**L. Poladian** is an Australian Research Council Professorial Fellow, working in the School of Mathematics and Statistics at the University of Sydney, Sydney, NSW, Australia. A "house-trained" theoretician, he works extensively with experimentalists in areas ranging from optical waveguide design and modeling to developing new evolutionary algorithms.

**R. Lwin** received the B.E. degree in Aeronautics and Space from the University of Sydney, Sydney, Australia, in 2004. He is currently working toward the Ph.D. degree with the Chemical Engineering Department and the Optical Fibre Technology Centre, University of Sydney, working on the fabrication and optimization of microstructured polymer optical fibres.